Efficient Recovery of Sub-Nyquist Sampled Sparse Multi-Band Signals Using Reconfigurable Multi-Channel Analysis and Modulated Synthesis Filter Banks

Anu Kalidas Muralidharan Pillai and Håkan Johansson

Anu Kalidas Muralidharan Pillai and Håkan Johansson, Efficient Recovery of Sub-Nyquist Sampled Sparse Multi-Band Signals Using Reconfigurable Multi-Channel Analysis and Modulated Synthesis Filter Banks, 2015, *IEEE Transactions on Signal Processing*, 64(19) pp. 5238-5249.

http://dx.doi.org/10.1109/TSP.2015.2451104

Efficient Recovery of Sub-Nyquist Sampled Sparse Multi-Band Signals Using Reconfigurable Multi-Channel Analysis and Modulated Synthesis Filter Banks

Anu Kalidas M. Pillai, *Student Member, IEEE,* and Håkan Johansson, *Senior Member, IEEE*

***Abstract*—Sub-Nyquist cyclic nonuniform sampling (CNUS) of a sparse multi-band signal generates a nonuniformly sampled signal. Assuming that the corresponding uniformly sampled signal satisfies the Nyquist sampling criterion, the sequence obtained via CNUS can be passed through a reconstructor to recover the missing uniform-grid samples. At present, these reconstructors have very high design and implementation complexity that offsets the gains obtained due to sub-Nyquist sampling. In this paper, we propose a scheme that reduces the design and implementation complexity of the reconstructor. In contrast to the existing reconstructors which use only a multi-channel synthesis filter bank (FB), the proposed reconstructor utilizes both analysis and synthesis FBs which makes it feasible to achieve an order-of-magnitude reduction of the complexity. The analysis filters are implemented using polyphase networks whose branches are allpass filters with distinct fractional delays and phase shifts. In order to reduce both the design and the implementation complexity of the synthesis FB, the synthesis filters are implemented using a cosine-modulated FB. In addition to the reduced complexity of the reconstructor, the proposed multi-channel recovery scheme also supports online reconfigurability which is required in flexible (multi-mode) systems where the user subband locations vary with time.**

***Index Terms*—Sub-Nyquist sampling, sparse multi-band signals, reconstruction, nonuniform sampling, time-interleaved analog-to-digital converters, filter banks.**

I. Introduction

It is well recognized that data acquisition (analog-to-digital conversion) constitutes one of the bottlenecks in signal processing and communication systems [1]. In particular, with the increasing demands for high data rates and resolution, the power consumption of the data acquisition is becoming intolerably high, especially in battery-powered wideband communication systems. An emerging research focus is therefore to utilize structures (sparsities) in the analog signals in order to reduce the average acquisition rate and thereby reduce the cost [2]–[5]. This is referred to as sub-Nyquist sampling of sparse signals which has the potential to dramatically reduce the power consumption. Typically, in uniform sampling, a signal that is bandlimited to $f < f_0$ is sampled at a rate of $f_s \geq 2f_0$. In sub-Nyquist sampling, the average sampling rate is lower than $2f_0$ but still large enough to capture the information content in the signal. There are essentially two paradigms within this area. The first covers multi-band (or multi-coset) sampling where the use of cyclic nonuniform sampling (CNUS) enables a reduction of the average sampling rate to (in principle) the Landau minimal sampling rate which is determined by the frequency occupancy [4], [6]. The other paradigm is compressive sampling (or compressed sensing) [4], [5] which in practice (so far) utilizes modulation with a (pseudo) random signal, integration, and low-rate uniform sampling. Both of these approaches have their own unique advantages and drawbacks and it is likely that both of them in the future will be employed but in different contexts depending on the application. In this paper, we are primarily interested in the CNUS approach.

For CNUS, the sub-Nyquist sampled signal is passed through a digital reconstructor to recover the uniformly spaced samples. Thus, assuming that the corresponding uniformly sampled signal satisfies the Nyquist sampling criterion, the sampling problem to be considered in this paper corresponds to the recovery of uniform-grid samples given a subset of those samples. Given K samples in each block (period) of M samples, ($K < M$), the problem is to recover the $M - K$ missing samples. For the CNUS approach, it is known that the reconstruction can be done, in principle, via a set of ideal multi-level synthesis filters, given the sampling pattern [7]–[9]. The related problem of selecting the optimal sampling patterns has also been addressed [9]–[11]. However, the straightforward CNUS recovery scheme has very high design and implementation complexities[1]. Also, in frequency-hopping communication systems where the active user band locations are different for different time frames, the reconstruction scheme should support online reconfigurability with low complexity. Further, it is noted that here, like in [7]–[9], we only consider the recovery of the uniform-grid samples corresponding to the entire sparse multi-band signal. In order to extract the uniform-grid signal corresponding to the frequency band of each active user, regular filtering can be used at the output of the reconstructor. Also, we assume that the location of the active subbands are known and available beforehand as in [7]–[9].

A. Contributions and Outline of the Paper

In this paper, we will introduce the efficient recovery scheme shown in Fig. 1, which is derived by first expressing the reconstructor design problem in terms of multi-channel analysis and synthesis filter banks (FBs). In this scheme, the

This work was supported by the Swedish Research Council (VR), ELLIIT, and Security-Link.

The authors are with the Division of Communication Systems, Department of Electrical Engineering, Linköping University, Linköping, Sweden (email: kalidas@isy.liu.se, hakanj@isy.liu.se).

[1]Typically, in reconstructor implementations, multipliers are the most expensive components in terms of area and power. Hence, in this paper we use the number of multiplications per corrected output sample as a measure of the computational complexity of the implementation.

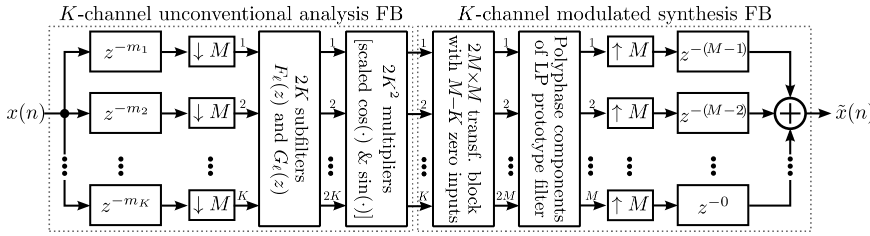

Fig. 1. Proposed efficient reconfigurable reconstructor. The scheme is derived using the concepts explained in Section IV.

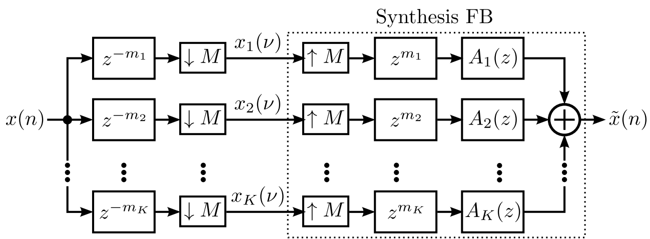

Fig. 2. Reconstruction using a set of multi-level synthesis filters [7].

synthesis FB consists of K regular bandpass filters which are implemented using a cosine-modulated FB. The analysis FB makes use of K unconventional bandpass filters. The bandpass filters are unconventional in the sense that they contain only K instead of M polyphase components. These polyphase components are allpass filters with distinct fractional delays and phase shifts and can be implemented based on polynomial impulse response filters. Due to this, there is no need for online filter design when the locations of the active subbands are changed to new positions. This is unlike in [7], which uses general multi-level synthesis filters that necessitate redesign for each new mode. Thus, the recovery scheme in [7], shown in Fig. 2, is costly and unattractive (or even unacceptable) in low-power applications like hand-held communication devices. In [8], the design complexity of the multi-level synthesis filters is reduced by using a polyphase FB. However, as pointed out in [8], other than for a few combinations of K and M, the design method in that paper offers no direct control on the magnitudes of the residual aliasing terms. It is also noted that there exist efficient reconstruction techniques for other types of nonuniformly sampled signals, like lowpass signals in time-interleaved analog-to-digital converters (TI-ADCs) [12]–[15], which belong to the class of undersampled multi-channel systems [16], [17], but those efficient recovery techniques are not applicable for the CNUS scheme considered here. Further, even though the reconstruction scheme in Fig. 2 can be obtained from generalized results like in [7], [16], these results cannot be straightforwardly used to derive the proposed scheme in Fig. 1.

Parts of this work have been presented at a conference [18] where only the basic concept was outlined without giving any proofs. However, in order to get further insight and understanding of the efficient reconfigurable scheme, in Section IV we show that the reconstruction problem can be expressed in terms of the proposed analysis and synthesis FBs. Based on this, we introduce a reconfigurable reconstruction scheme in Section V. Using complexity expressions for the proposed reconstructor and the polyphase implementation of the straightforward scheme in [7], we show that order-of-magnitude reduction of the complexity is achievable using the proposed reconstructor. Furthermore, in [18], the filters in the analysis FB were designed using numerical optimization which can be time-consuming especially for higher filter orders and/or larger K. In Section VI of this paper, we propose a least-squares approach for designing these filters so that their filter coefficients can be obtained via a closed-form solution. In addition to reducing the design effort, the closed-form solution enables us to redetermine the filter coefficients online, if required. Also, in Section VII, we use detailed design examples to show that the proposed method offers significant complexity savings, particularly for larger M. In order to provide the necessary background for the above mentioned sections, in Section III we review the concept of sub-Nyquist CNUS of sparse multi-band signals. Immediately following this introduction, in Section II, we define the notations used in this paper as well as briefly review some of the signal processing concepts that will be used in later sections.

II. Preliminaries

A. Notations

Bold lowercase letters are used to denote vectors while bold uppercase letters are used to denote matrices. Transpose and conjugate-transpose are represented using $(\cdot)^T$ and $(\cdot)^\dagger$, respectively. For a filter with impulse response coefficients $h(n)$, we use $H(z)$ to denote its transfer function which is defined as $H(z) = \sum_n h(n)z^{-n}$. The frequency response of the filter is denoted by $H(e^{j\omega})$ and is obtained from the transfer function by replacing z with $e^{j\omega}$.

B. Polyphase Decomposition

Any filter $H(z)$ can generally be expressed in terms of its polyphase components $H_m(z)$, $m = 0, 1, \ldots, M-1$, as [19], [20]

$$H(z) = \sum_{m=0}^{M-1} z^{-m} H_m(z^M). \tag{1}$$

Polyphase decomposition as in (1) along with the noble identities shown in Fig. 3 [20], can be used to derive efficient structures for decimation and interpolation. For example, consider the decimator shown in Fig. 4(a). Expressing $H(z)$ in Fig. 4(a) as in (1) and then propagating the downsampler to the left using the noble identity shown in Fig. 3(a), we get the

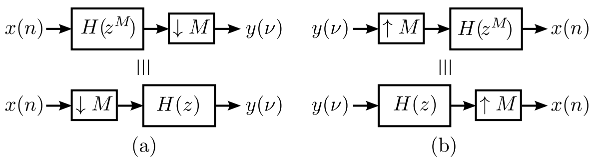

Fig. 3. Noble identities.

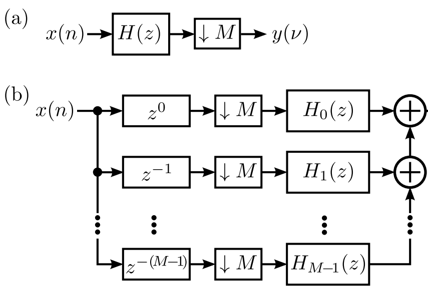

Fig. 4. (a) Decimator. (b) Equivalent representation of (a) using the M polyphase branches of the filter $H(z)$.

polyphase structure in Fig. 4(b). It can be seen that, unlike in Fig. 4(a), in the polyphase structure the filtering takes place at the lower rate. It is noted that the corresponding polyphase structure for the interpolator can be obtained by transposing the structure in Fig. 4(b) and replacing each downsampler with an upsampler [20].

C. Generalized Fractional-Delay Filter

A generalized fractional-delay (FD) filter has a phase shift in addition to the fractional delay [21] and its frequency response can be expressed as

$$H(e^{j\omega}) = e^{j(\omega d + \alpha \operatorname{sgn}(\omega))}, \ \omega \in [-\pi, \pi] \tag{2}$$

with $d, \alpha \in \mathbb{R}$. Here, d represents the fractional delay, α is the additional phase shift, and $\operatorname{sgn}(\omega)$ denotes the sign of ω.

III. Sub-Nyquist Cyclic Nonuniform Sampling of Sparse Multi-Band Signals

Assume that $x_a(t)$ is a real-valued continuous-time signal that carries information within the frequency band $\omega \in (-2\pi f_0, 2\pi f_0)$, $f_0 < 1/(2T)$. Uniform sampling of $x_a(t)$ at a sampling frequency of $f_s = 1/T$ results in a discrete-time sequence $x(n) = x_a(nT)$. Below, for the sake of simplicity, we assume that $T = 1$. Now it is assumed that the band $\omega \in [0, \pi]$ is divided into M granularity bands of equal width π/M. In sparse multi-band signals, at any given time frame, only K of the M granularity bands ($K < M$) are allocated to users. In this paper, $r_i \in [0, 1, \ldots, M-1]$, $i = 1, 2, \ldots, K$, denote the active granularity bands. Figure 5 shows the principle spectrum of a sparse multi-band signal when $M = 16$, $K = 3$, and with active granularity bands $r_{1,2,3} = [1, 4, 10]$. A user can occupy one or several consecutive granularity bands. Further, to be able to design practical filters, we assume a certain amount of redundancy (oversampling) which corresponds to transition bands between user bands. In case of such sparse multi-band signals, uniform sampling will generate

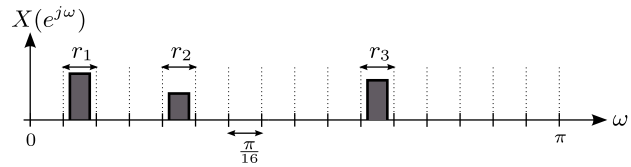

Fig. 5. Spectrum of a sparse multi-band signal with $M = 16$ and $K = 3$.

more samples than what is required to prevent information loss. The number of samples generated during the sampling process can be reduced by using CNUS which only uses a subset of the uniform samples $x(n)$, i.e., $x(Mn - m_\ell)$, $\ell = 1, 2, \ldots, K$ with $m_\ell \in [0, 1, \ldots, M-1]$. It can be viewed as if the available input samples $x_\ell(\nu) = x(M\nu - m_\ell)$, $\ell = 1, 2, \ldots, K$, $\nu \in \mathbb{Z}$, are obtained from the uniform-grid samples $x(n)$ as shown in Fig. 2. A practical implementation of the CNUS is an M-channel TI-ADC [22] where only a subset of the channels are used[2]. A reconstructor can then be used to recover the uniformly sampled sequence $x(n)$ from $x_\ell(\nu)$, $\ell = 1, 2, \ldots, K$, for a given set of K granularity bands, provided the sampling instants m_ℓ are selected properly [11].

A reconstruction scheme using multi-level synthesis filters $A_\ell(z)$, $\ell = 1, 2, \ldots, K$, as shown in Fig. 2, was proposed in [7]. It was shown that perfect reconstruction, i.e., $\tilde{x}(n) = x(n)$, can be achieved in principle using ideal multi-level synthesis filters $A_\ell(z)$. Perfect reconstruction (PR) is generally not feasible with realizable filters. However, in practice, it is sufficient to determine $A_\ell(z)$ such that PR is approximated within a given tolerance. This can be carried out by designing $A_\ell(z)$ straightforwardly, assuming no a priori relations between the filters. However, the reconstructor thus designed may become intolerably costly in real-time applications as the computational complexity of this approach is roughly $N_A K/M$ multiplications per corrected output sample, where N_A is the filter order of $A_\ell(z)$. Also, at a later time frame, if the location of the K bands change, then all $A_\ell(z)$ need redesign. The design complexity of $A_\ell(z)$ is high as regular filter design with many unknowns is too computationally intensive and time consuming to be carried out online.

IV. Proposed Reconstruction Using Analysis and Synthesis FBs

In this paper, to reduce the complexity, we describe the reconstruction in terms of both analysis and synthesis filters as shown in Fig. 6. Expressing the reconstruction in terms of analysis and synthesis filters as shown in Fig. 6 enables efficient implementation of the overall reconstructor (to be considered in Section V). The complexity reduction is due to the fact that the synthesis filters $C_k(z)$ can be efficiently realized using a cosine-modulated FB whereas a common set of fixed subfilters can be utilized to implement all the filters $B_k(z)$ in the analysis FB as shown in the proposed reconstructor in Fig. 1. It will be shown below that the

[2] Like in [7], the proposed reconstructor can be extended to use noninteger values for m_ℓ. However, since practical implementations of CNUS schemes make use of TI-ADCs, we assume m_ℓ to be an integer as this appears to be the preferred choice.

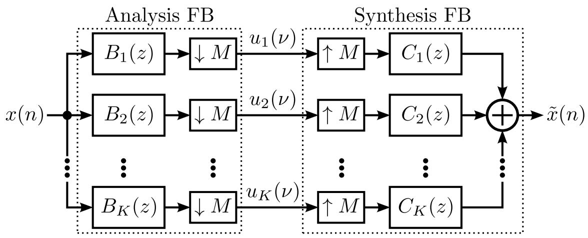

Fig. 6. Reconstruction of sub-Nyquist sampled sparse multi-band signal using analysis and synthesis filters.

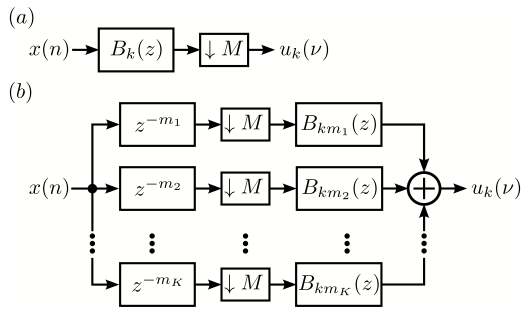

Fig. 7. (a) Bandpass decimator in the kth branch of the analysis FB in the proposed reconstructor. (b) Equivalent representation of (a) when $x_\ell(\nu)$, the available samples in $x(n)$, are obtained via sub-Nyquist CNUS as in Fig. 2. Due to the CNUS, only the inputs to K polyphase branches of the bandpass filter $B_k(z)$ are non-zero.

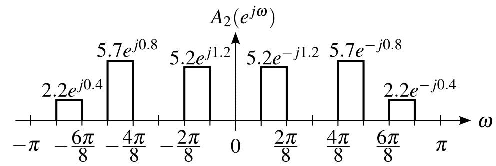

Fig. 8. Frequency response of the ideal multi-level synthesis filter $A_2(z)$ in [7] for $M = 8$, $K = 3$, and $r_{1,2,3} = [1, 4, 6]$. The sampling instants are $m_{1,2,3} = [0, 3, 5]$.

synthesis filters $C_k(z)$ are K different conventional bandpass filters whereas each analysis filter $B_k(z)$ is an unconventional bandpass filter with only K non-zero polyphase components. Also, it will be shown that the filters $B_k(z)$ and $C_k(z)$, $k \in 1, 2, \ldots, K$, correspond to the active granularity band r_k.

A. Unconventional Bandpass Filters

Figure 7(a) shows the kth branch of the analysis FB in the proposed reconstructor. Using polyphase decomposition defined in Section II-B, the filter $B_k(z)$ can be expressed in terms of its M polyphase components $B_{km}(z)$, $m = 0, 1, \ldots, M-1$, as

$$B_k(z) = \sum_{m=0}^{M-1} z^{-m} B_{km}(z^M). \tag{3}$$

Recall from Section III that the available samples in $x(n)$, i.e., $x_\ell(\nu)$, $\ell = 1, 2, \ldots, K$, are obtained via sub-Nyquist CNUS as shown in Fig. 2. Thus it can be seen that, due to the missing samples in $x(n)$, the inputs to $M - K$ polyphase branches of the bandpass filter $B_k(z)$ in Fig. 7(a) will be equal to zero. This implies that, for the CNUS scheme, (3) reduces to

$$B_k(z) = \sum_{\ell=1}^{K} z^{-m_\ell} B_{km_\ell}(z^M) \tag{4}$$

where $m_\ell \in [0, 1, \ldots, M-1]$, $\ell = 1, 2, \ldots, K$, are the K sampling instants and $B_{km_\ell}(z)$ are the K non-zero polyphase components of $B_k(z)$. Hence, the bandpass decimator in Fig. 7(a) can be redrawn as shown in Fig. 7(b). It is noted that conventional bandpass filters can be considered as a special case of the unconventional bandpass filter when all the samples in $x(n)$ are available. We will now state the expression for the non-zero polyphase components in the following theorem.

Theorem 1: In the proposed reconstructor in Fig. 6, the non-zero polyphase components $B_{km_\ell}(e^{j\omega})$, $m_\ell \in [0, 1, \ldots, M-1]$, $\ell = 1, 2, \ldots, K$, of the unconventional bandpass filter $B_k(e^{j\omega})$, $k \in [1, 2, \ldots, K]$, in (4) are generalized FD filters given by

$$B_{km_\ell}(e^{j\omega}) = \frac{\beta_{km_\ell}}{M} e^{j(\omega m_\ell/M + \alpha_{km_\ell}\,\mathrm{sgn}(\omega))}, \;\; \omega \in [-\pi, \pi] \tag{5}$$

with $\beta_{km_\ell}, \alpha_{km_\ell} \in \mathbb{R}$.

Proof. In order to prove Theorem 1 we show that, with $B_{km_\ell}(e^{j\omega})$ as in (5), the reconstructor in Fig. 2 [7] is equivalent to the proposed reconstructor in Fig. 6. In the following derivation, we assume as in [7] that the reconstruction of a sub-Nyquist sampled signal with K active bands is performed using ideal synthesis filters $A_\ell(z)$, $\ell = 1, 2, \ldots, K$. As can be seen from Fig. 8, the frequency response of each synthesis filter $A_\ell(z)$, $\ell \in 1, 2, \ldots, K$, has non-zero levels in the occupied granularity bands $r_i \in [0, 1, \ldots, M-1]$, $i = 1, 2, \ldots, L$, and is zero elsewhere. In the granularity band r_k, the frequency response of the synthesis filter $A_\ell(z)$ is given by

$$A_\ell(e^{j\omega}) = \frac{1}{M} \beta_{km_\ell} e^{j\alpha_{km_\ell}\,\mathrm{sgn}(\omega)} C_k(e^{j\omega}) \tag{6}$$

where $\omega \in \{[-(r_k+1)\pi/M, -r_k\pi/M] \cup [r_k\pi/M, (r_k+1)\pi/M]\}$, $C_k(e^{j\omega})$ is a bandpass filter with passband at the granularity band r_k so that

$$C_k(e^{j\omega}) = \begin{cases} M, & \omega \in \{[\frac{-(r_k+1)\pi}{M}, \frac{-r_k\pi}{M}] \cup [\frac{r_k\pi}{M}, \frac{(r_k+1)\pi}{M}]\} \\ 0, & \text{elsewhere} \end{cases}, \tag{7}$$

and β_{km_ℓ}, α_{km_ℓ} are the modulus and angle, respectively, of the complex constant υ_{km_ℓ} that correspond to the level of $A_\ell(e^{j\omega})$ in the band r_k. Considering the contributions from all the synthesis filters $A_\ell(e^{j\omega})$, $\ell = 1, 2, \ldots, K$, to the overall frequency response in the granularity band r_k, the structure in Fig. 2 can be redrawn for the band r_k as shown in Fig. 9(a) where

$$B_{km_\ell}(e^{j\omega M}) = \frac{1}{M} \beta_{km_\ell} e^{j(\omega m_\ell + \alpha_{km_\ell}\,\mathrm{sgn}(\omega))}. \tag{8}$$

The term $e^{j\omega m_\ell}$ in (8) corresponds to z^{m_ℓ} in Fig. 2. Using the noble identities [20] shown in Fig. 3 to propagate each $B_{km_\ell}(e^{j\omega M})$ in Fig. 9(a) to the left through the upsample

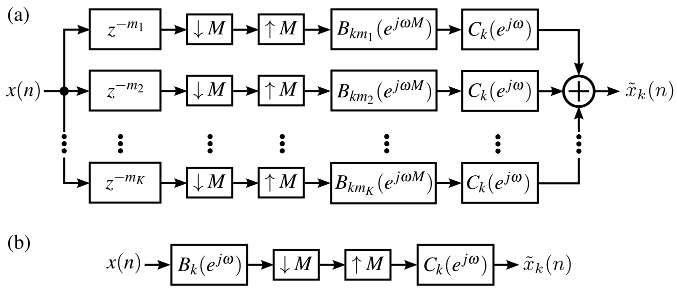

Fig. 9. (a) FB representation of the reconstructed signal in the granularity band r_k. (b) Simplified representation of (a) where each $B_{km_\ell}(e^{j\omega})$ in (a) are the m_ℓth polyphase component of $B_k(e^{j\omega})$.

and downsample blocks, we get the simplified representation shown in Fig. 9(b) where

$$B_k(e^{j\omega}) = \sum_{\ell=1}^{K} e^{-j\omega m_\ell} B_{km_\ell}(e^{j\omega M}). \tag{9}$$

Now, the output of the reconstructor is obtained by adding the outputs from all the K bands. That is, $\tilde{x}(n)$ in Fig. 2 is given by

$$\tilde{x}(n) = \sum_{k=1}^{K} \tilde{x}_k(n). \tag{10}$$

Thus, using the representation in Fig. 9(b) for each of those granularity bands, we can see that the FB representation using ideal synthesis filters in Fig. 2 is equivalent to that of the proposed FB structure in Fig. 6 with the non-zero polyphase components of $B_k(e^{j\omega})$ as in (5). $\square$

From the above discussion it is noted that, in the proposed reconstructor, the analysis filter $B_k(z)$ extracts the signal in the active granularity band r_k. The filtering by $B_k(z)$ is followed by downsampling by M so as to have the extracted granularity band r_k at the lower sampling rate f_s/M. The low-rate signal is then placed at the original granularity band location r_k at the higher rate f_s via upsampling by M followed by bandpass filtering via $C_k(z)$.

B. Determining β_{km_ℓ} and α_{km_ℓ}

Next, we will show that the constants β_{km_ℓ} and α_{km_ℓ}, $\ell = 1, 2, \ldots, K$, $m_\ell \in [0, 1, \ldots, M-1]$, for all the bandpass filters $B_k(z)$, $k = 1, 2, \ldots, K$, can be determined through a single $K \times K$ matrix inversion.

Theorem 2: Consider the bandpass filters $B_k(z)$, $k = 1, 2, \ldots, K$, which extract the active subbands $r_k \in [0, 1, \ldots, M-1]$, $k = 1, 2, \ldots, K$, respectively. Let $\mathbf{v}_k$ be a vector ($K \times 1$ matrix) containing all the K complex constants υ_{km_ℓ} corresponding to the non-zero polyphase components of $B_k(z)$, $k \in [1, 2, \ldots, K]$. Then, $\mathbf{v}_k$ can be determined using matrix inversion as

$$\mathbf{v}_k = \mathbf{D}^{-1}\mathbf{b}_k \tag{11}$$

where $\mathbf{D}$ is a $K \times K$ generalized Vandermonde matrix given by

$$\mathbf{D} = \frac{1}{M}\begin{bmatrix} e^{j2\pi q_1 m_1/M} & e^{j2\pi q_1 m_2/M} & \ldots & e^{j2\pi q_1 m_K/M} \\ e^{j2\pi q_2 m_1/M} & e^{j2\pi q_2 m_2/M} & \ldots & e^{j2\pi q_2 m_K/M} \\ \vdots & \vdots & \ddots & \vdots \\ e^{j2\pi q_K m_1/M} & e^{j2\pi q_K m_2/M} & \ldots & e^{j2\pi q_K m_K/M} \end{bmatrix} \tag{12}$$

and $\mathbf{b}_k$ is a vector ($K \times 1$ matrix) containing $K-1$ zeros and unity for the position k. In (12), $q_i \in [0, 1, \ldots, M-1]$, $i = 1, 2, \ldots, K$, depend on the corresponding active subband locations $r_i \in [0, 1, \ldots, M-1]$ and is given by

$$q_i = \begin{cases} \frac{r_i+1}{2}, & \text{odd } r_i \\ M - \frac{r_i}{2}, & \text{even } r_i \neq 0 \\ 0, & r_i = 0 \end{cases}. \tag{13}$$

Proof. We divide the frequency range $[-\pi/M,\ 2\pi - \pi/M]$ into M adjacent regions of equal width $2\pi/M$ as shown in Fig. 10(a). Thus, region p, $p \in [0, 1, \ldots, M-1]$, covers the frequencies in $[-\pi/M + 2\pi p/M,\ -\pi/M + 2\pi(p+1)/M]$. The passband of the desired bandpass filter $B_k(e^{j\omega})$ covers the band $\omega \in [r_k\pi/M,\ (r_k+1)\pi/M]$ and thus also $\omega \in [2\pi - (r_k+1)\pi/M,\ 2\pi - r_k\pi/M]$ as shown in Fig. 10(b). Further, comparing Figs. 10(a) and 10(b), we can see that if an active subband r_i, $i \in [1, 2, \ldots, K]$, occupies the left (right) half of a region p, it will also occupy the right (left) half of the region $M - p$.

Next, we make use of the fact that the non-zero polyphase components $B_{km_\ell}(e^{j\omega})$ in (5) are 2π-periodic with respect to ω. This implies that $B_{km_\ell}(e^{j\omega}) = B_{km_\ell}(e^{j(\omega - 2\pi p)})$ for $\omega \in [-\pi + 2\pi p,\ -\pi + 2\pi(p+1)]$, $\forall p \in \mathbb{Z}$. It is further noted that $B_{km_\ell}(e^{j\omega M})$ are compressed (by M) versions of the corresponding frequency responses $B_{km_\ell}(e^{j\omega})$. This means that $B_{km_\ell}(e^{j\omega M})$ for $\omega \in [-\pi/M + 2\pi p/M,\ -\pi/M + 2\pi(p+1)/M]$ equals $B_{km_\ell}(e^{j\omega})$ for $\omega \in [-\pi + 2\pi p,\ -\pi + 2\pi(p+1)]$. Due to the $\operatorname{sgn}(\omega)$ in (5), $B_{km_\ell}(e^{j\omega M}) = \beta_{km_\ell} e^{j(\omega m_\ell - 2\pi p m_\ell/M - \alpha_{km_\ell})}/M$ in the left part of region p whereas $B_{km_\ell}(e^{j\omega M}) = \beta_{km_\ell} e^{j(\omega m_\ell - 2\pi p m_\ell/M + \alpha_{km_\ell})}/M$ in the right part of the same region. Using these expressions in (4), for $\omega \in [-\pi/M + 2\pi p/M,\ 2\pi p/M]$ (left part of region p), we get[3]

$$B_k(e^{-j\omega}) = \frac{1}{M}\sum_{\ell=1}^{K} \beta_{km_\ell} e^{j\alpha_{km_\ell}} e^{j2\pi p m_\ell/M} \tag{14}$$

and for $\omega \in [2\pi p/M,\ -\pi/M + 2\pi(p+1)/M]$ (right part of region p), we obtain

$$B_k(e^{j\omega}) = \frac{1}{M}\sum_{\ell=1}^{K} \beta_{km_\ell} e^{j\alpha_{km_\ell}} e^{-j2\pi p m_\ell/M}. \tag{15}$$

It can be seen that (14) and (15) also correspond to the right and left half, respectively, of region $M - p$. Thus, if $q_i \in [0, 1, \ldots, M-1]$, given as in (13), represent the region whose left half is occupied by the active subband r_i, then

[3]In (14), we used $B_k(e^{-j\omega})$ since real filters are assumed. For real filters, $B_k(e^{j\omega}) = 1$ ($B_k(e^{j\omega}) = 0$) in the passband (stopband) region implies $B_k(e^{-j\omega}) = 1$ ($B_k(e^{-j\omega}) = 0$) as well.

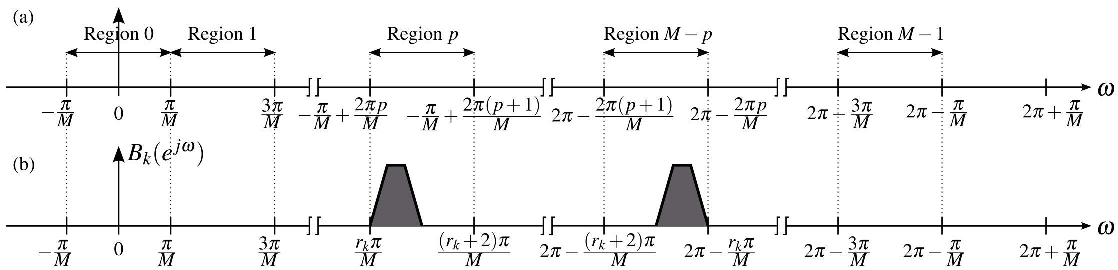

Fig. 10. (a) Illustrates of the division of the frequency range $[-\pi/M,\ 2\pi-\pi/M]$ into M adjacent regions of equal width $2\pi/M$. (b) Spectrum of a bandpass filter $B_k(e^{j\omega})$ with passband in the frequency range $[r_k\pi/M,\ (r_k+1)\pi/M]$.

the requirement on $B_k(e^{j\omega})$ in q_i is equal to the requirement in the right half of the region $M-q_i$. Consequently, for the bandpass filter $B_k(e^{j\omega})$ it suffices to solve a system of K equations corresponding to the left half of the K regions q_i, $i=1,2,\ldots,K$. More precisely, the right hand side of (14) should equal unity in the region q_k and zero in the $K-1$ regions q_i, $i\in[1,2,\ldots,K]$, $i\neq k$. Thus, using $\upsilon_{km_\ell}=\beta_{km_\ell}e^{j\alpha_{km_\ell}}$ in (14), we obtain the system of equations

$$\mathbf{D}\mathbf{v}_k=\mathbf{b}_k \tag{16}$$

where

$$\mathbf{v}_k=[\upsilon_{km_1}\ \upsilon_{km_2}\ \ldots\ \upsilon_{km_K}]^T. \tag{17}$$

The vector $\mathbf{v}_k$ corresponding to the bandpass filter $B_k(e^{j\omega})$ can then be determined using (11). □

Theorem 2 shows that the vectors $\mathbf{v}_k$ corresponding to all the K bandpass filters $B_k(e^{j\omega})$, $k=1,2,\ldots,K$, can be determined by inverting a single $K\times K$ matrix. Also, consistent with the results in [7], it can be seen from (12) that there is always at least one set of sampling instants that corresponds to an invertible matrix, namely $m_\ell=0,1,\ldots,K$, since for these sampling points the generalized Vandermonde matrix $\mathbf{D}$ reduces to a Vandermonde matrix. However, these sampling instants may not guarantee that the matrix $\mathbf{D}$ is well conditioned. In order to ensure that $\mathbf{D}$ is well conditioned, optimal sampling instants can be selected depending on the active subband locations as outlined in [9], [11].

V. Proposed Efficient Reconstructor

Using the reconstruction scheme described in Section IV, we will now derive the proposed efficient reconfigurable reconstructor shown in Fig. 1.

A. Synthesis and Analysis FBs

In order to implement the cosine-modulated synthesis FB, a lowpass filter with cutoff frequency at $\pi/2M$ is used as the prototype filter $P(z)$ [20]. The coefficients of the synthesis filters $c_k(n)$ can be expressed in terms of the impulse response of the prototype filter $\wp(n)$ as [20]

$$c_k(n)=2M\wp(n)\cos\left(\frac{\pi}{M}(k+0.5)(n-\frac{N_P}{2})-(-1)^k\frac{\pi}{4}\right). \tag{18}$$

The overall complexity of the synthesis FB correspond to that of the prototype filter plus the cost of a real or complex transform block. By using a fast-transform algorithm, the cost of such a transform block can be made small when compared to the cost of the filters.

In the analysis FB, since the polyphase components of each $B_k(z)$ are as given in (5), all the analysis filters can be expressed with a common set of fixed subfilters, $F_\ell(z)$ and $G_\ell(z)$, $\ell=1,2,\ldots,K$. The different analysis filters are then obtained via different pairs of values of β_{km_ℓ} and $\theta_{km_\ell}=\alpha_{km_\ell}+\pi/4$ such that

$$B_{km_\ell}(z)=\frac{\beta_{km_\ell}}{M}[\cos(\theta_{km_\ell})F_\ell(z)+\sin(\theta_{km_\ell})G_\ell(z)] \tag{19}$$

where

$$F_\ell(e^{j\omega})\approx e^{j\omega m_\ell/M},\ \ G_\ell(e^{j\omega})\approx \mathrm{sgn}(\omega)\times je^{j\omega m_\ell/M}. \tag{20}$$

It is noted that the additional phase of $\pi/4$ in θ_{km_ℓ} is required to ensure proper matching between adjacent analysis and synthesis filters in the case of overlapping granularity bands and when cosine-modulated synthesis FB is used. This is similar to the additional constants used for matching in conventional cosine-modulated FBs [20]. However, the additional constant used in θ_{km_ℓ} is $\pi/4$ instead of $(-1)^k\pi/4$ which is used in conventional cosine-modulated FBs. This is because, in the proposed reconstructor, the additional phase constants are applied on the polyphase components of the analysis filter. In conventional cosine-modulated FBs, the additional phase constants are applied on the overall analysis and synthesis filters as in (18).

B. Computational Complexity

In this paper we consider computational complexity as the number of real multiplications required per corrected output sample (see Footnote 1). Based on the discussions above, and polyphase realizations in which all the filtering takes place at the downsampled rate, the computational complexity of the proposed reconstructor in Fig. 1 can be approximated as

$$\mathcal{C}_{\text{prop}}\approx\frac{N_P}{M}+\log_2(M)+\frac{2N_FK}{M}+\frac{2K^2}{M}. \tag{21}$$

In (21), N_P is the order of the prototype filter for the synthesis FB and N_F is the order of the fixed subfilters $F_\ell(z)$ and $G_\ell(z)$. The first two terms in the expression for $\mathcal{C}_{\text{prop}}$ in (21), correspond to the computational complexity of the cosine-modulated synthesis FB assuming that the $2M\times M$ transform block is implemented using a fast-transform algorithm [23].

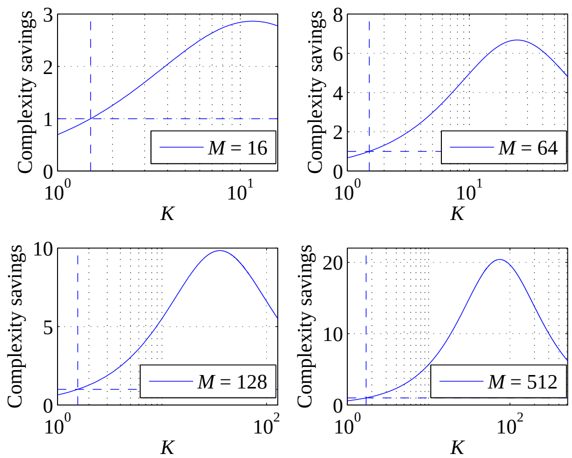

Fig. 11. Illustration of the estimated complexity savings of the proposed scheme compared to the polyphase implementation of the straightforward scheme [7] (Complexity savings = $\mathcal{C}_{\text{reg}}/\mathcal{C}_{\text{prop}}$).

The third term is the computational complexity of the $2K$ subfilters $F_\ell(z)$ and $G_\ell(z)$ whereas the fourth term corresponds to the complexity of the $2K^2$ multipliers whose coefficients are the scaled $\cos(\cdot)$ and $\sin(\cdot)$ terms in (19). Typically, N_P is about an order of magnitude larger than M as explained below. An approximate estimate of the order of the prototype filter, N_P, is given by [24]

$$N_P \approx -\frac{2}{3}\log_{10}(10\delta_c\delta_s)\frac{2\pi}{\omega_s-\omega_c} \tag{22}$$

where δ_c, δ_s, ω_c, and ω_s denote the passband ripple, stopband ripple, passband edge, and stopband edge, respectively, of the prototype filter. Assuming that ρ is the percentage occupancy of a granularity band, for a prototype filter with transition band centered at $\pi/2M$, $\omega_s-\omega_c=\varepsilon\pi/M$ where $\varepsilon=1-\rho/100$. For example, if ρ varies between 20–60%, for a prototype filter with passband and stopband ripple of -60 dB, N_P will be between $9M$–$17M$. Also, the order of the subfilters $F_\ell(z)$ and $G_\ell(z)$ is $N_F\approx N_P/M$. The complexity of the polyphase implementation of the straightforward scheme in Fig. 2 can be estimated as

$$\mathcal{C}_{\text{reg}} \approx \frac{N_P K}{M}. \tag{23}$$

As exemplified in Fig. 11, which plots the ratio $\mathcal{C}_{\text{reg}}/\mathcal{C}_{\text{prop}}$ for $N_P=13M$ and $N_F=N_P/M$, order-of-magnitude savings are feasible, via proper choices of M and K (also see Example 1 in Section VII for a specific example).

C. *Reconfiguration Complexity*

In the proposed reconstructor, the real-time reconfiguration is simple and fast as it suffices to determine the multiplier values β_{km_ℓ} and θ_{km_ℓ} using (11). Thus, during reconfiguration, only the coefficients of the $2K^2$ multipliers corresponding to the scaled $\cos(\cdot)$ and $\sin(\cdot)$ terms in (19) need to be updated. As explained in Section VI below, the subfilters $F_\ell(z)$ and $G_\ell(z)$, as well as the prototype filter for the cosine-modulated synthesis FB, are designed once offline and are fixed in the implementation. Due to this, all the multipliers in the cosine-modulated FB as well as in the fixed subfilters can be implemented using fixed-coefficient multipliers. This helps to reduce the overall implementation complexity since, compared to variable-coefficient multipliers, efficient techniques can be used to implement the fixed-coefficient multipliers [25], [26]. Moreover, using a common set of fixed subfilters to implement all the analysis filters $B_k(z)$, $k=1,2,\dots,K$, results in fewer design variables which helps to reduce the design complexity of the analysis FB.

VI. Design of the Proposed Reconstructor

In this section, we introduce a procedure to design the proposed reconstructor. Here, we assume that the sampling instants m_ℓ, $\ell=1,2,\dots,K$, are selected such that for the given active subbands r_k, $k=1,2,\dots,K$, $\mathbf{D}$ in (11) is an invertible matrix. Using the analysis and the synthesis FB representation in Fig. 6 for the proposed reconstruction scheme, the Fourier transform of the reconstructed output can be written as

$$Y(e^{j\omega}) = V_0(e^{j\omega})X(e^{j\omega}) + \sum_{\xi=1}^{M-1} V_\xi(e^{j\omega})X(e^{j(\omega-2\pi\xi/M)}) \tag{24}$$

where $V_0(e^{j\omega})$ is the *distortion function* and $V_\xi(e^{j\omega})$, $\xi = 1,2,\dots,M-1$, are the *aliasing functions* with

$$V_\xi(e^{j\omega}) = \frac{1}{M}\sum_{k=1}^{K} B_k(e^{j(\omega-2\pi\xi/M)})C_k(e^{j\omega}) \tag{25}$$

for $\xi=0,1,\dots,M-1$. As can be seen from (24) and (25), the analysis and synthesis filters should be designed such that the distortion and aliasing functions approximate unity and zero, respectively, in the active subband locations. The overall design complexity becomes very high if the subfilters $F_\ell(e^{j\omega})$ and $G_\ell(e^{j\omega})$ in (19) and the prototype filter for the cosine-modulated synthesis FB are designed together. Therefore, to reduce the overall design complexity, we propose the following design procedure. First, the prototype filter $P(e^{j\omega})$ is designed and fixed. Next, the coefficients of the $2K$ subfilters $F_\ell(e^{j\omega})$ and $G_\ell(e^{j\omega})$ are determined such that the distortion and aliasing terms are kept below a certain desired level. Due to the large number of constraints that need to be satisfied during the optimization, we use a least-squares approach so that the subfilter coefficients can be obtained via a closed-form solution. Compared to numerical optimization, such a closed-form solution significantly reduces the design time. Also, during reconfiguration, if a new set of sampling instants are selected, the closed-form solution makes it feasible to redetermine the coefficients online.

A. *Prototype Filter Design*

The prototype filter $P(e^{j\omega})$ is a power-symmetric lowpass filter with a passband edge at $\omega_c=(1-\varepsilon)\pi/2M$ and a stopband edge at $\omega_s=(1+\varepsilon)\pi/2M$ with ε related to the percentage occupancy ρ of the subband as $\varepsilon=1-\rho/100$. Due to the power-symmetry constraints as in (26) below, it is not possible to use a least-squares approach for the design of $P(e^{j\omega})$. However, unlike the design of the $2K$ subfilters $F_\ell(e^{j\omega})$ and $G_\ell(e^{j\omega})$, the prototype filter can be designed using numerical optimization techniques as the optimization has fewer constraints. Also, the coefficients of $P(e^{j\omega})$ are determined offline and only once, since the same $P(e^{j\omega})$ can be used even if the sampling instants change. In the subsequent design examples section, we use the MATLAB minimax optimization function `fminimax` for the design of $P(e^{j\omega})$. Using minimax design, the coefficients of $P(e^{j\omega})$ are determined such that the prototype filter approximates the passband and the stopband responses with unity and zero, respectively, as well as the power-symmetry property in the transition band with tolerances δ_0, δ_1, and δ_2 according to[4]

$$\begin{aligned} |P(e^{j\omega})-1| &\le \delta_0,\ \ \omega\in[0,\ \omega_c]\\ |P(e^{j\omega})| &\le \delta_1,\ \ \omega\in[\omega_s,\ \pi]\\ |1-|P(e^{j\omega})|^2-|P(e^{j(\omega-\pi/M)})|^2| &\le \delta_2,\ \ \omega\in[\omega_c,\ \omega_s]. \end{aligned} \tag{26}$$

The coefficients of $P(e^{j\omega})$ can therefore be obtained by solving the minimax optimization problem:

Given the order of the prototype filter N_P, determine the coefficients $\wp(n)$ of the prototype filter $P(e^{j\omega})$ and a parameter δ, to minimize δ subject to

$$\begin{aligned} |P(e^{j\omega})-1| &\le \delta,\ \ \omega\in[0,\ \omega_c]\\ |P(e^{j\omega})| &\le \delta,\ \ \omega\in[\omega_s,\ \pi]\ .\\ |1-|P(e^{j\omega})|^2-|P(e^{j(\omega-\pi/M)})|^2| &\le \delta,\ \ \omega\in[\omega_c,\ \omega_s] \end{aligned} \tag{27}$$

The filter $P(e^{j\omega})$ designed by solving the above optimization problem satisfies (26) if, after the optimization, $\delta \le \min(\delta_0,\delta_1,\delta_2)$. A good initial solution for the optimization problem can be obtained using, for example, the methods in [27], [28]. Our experiments indicate that δ should be 6–8 dB lower than the specified amplitude of the residual aliasing terms after reconstruction.

B. Least-Squares Design of $F_\ell(z)$ and $G_\ell(z)$

After determining the coefficients of the lowpass prototype filter for the synthesis FB, we use a least-squares approach to determine the coefficients of the fixed subfilters $F_\ell(z)$ and $G_\ell(z)$. The coefficients are determined such that they minimize an error power function $\mathcal{P}$ defined as

$$\mathcal{P}=\mathcal{P}_0+\sum_{\xi=1}^{M-1}\mathcal{P}_\xi \tag{28}$$

where

$$\mathcal{P}_0=\frac{1}{2\pi}\int_\Omega |V_0(e^{j\omega})-1|^2\,\mathrm{d}\omega,\ \ \Omega\in\Omega_{r_i,0} \tag{29}$$

and

$$\mathcal{P}_\xi=\frac{1}{2\pi}\int_\Omega |V_\xi(e^{j\omega})|^2\,\mathrm{d}\omega,\ \ \Omega\in\Omega_{r_i,\xi} \tag{30}$$

with $\Omega_{r_i,0}$, $r_i\in[0,1,\dots,M-1]$, $i=1,2,\dots,K$, representing the active subband locations and $\Omega_{r_i,\xi}$, $\xi=1,\dots,M-1$ represent the $2\pi\xi/M$-shifted versions of the active subbands that fall into the band $[-\pi,\pi]$. Let

$$\mathbf{h}=[\mathbf{f}_1\ \ \mathbf{g}_1\ \ \mathbf{f}_2\ \ \mathbf{g}_2\ \ \cdots\ \ \mathbf{f}_K\ \ \mathbf{g}_K]^T \tag{31}$$

where $\mathbf{f}_\ell$ and $\mathbf{g}_\ell$, $\ell=1,2,\dots K$, are the impulse response vectors of $F_\ell(e^{j\omega})$ and $G_\ell(e^{j\omega})$, respectively. In order to simplify the derivations, we assume that the order of the subfilters, N_F, is even such that

$$\mathbf{f}_\ell=[f_\ell(-N_F/2)\ \ f_\ell(-N_F/2+1)\ \ \cdots\ \ f_\ell(N_F/2)] \tag{32}$$

and

$$\mathbf{g}_\ell=[g_\ell(-N_F/2)\ \ g_\ell(-N_F/2+1)\ \ \cdots\ \ g_\ell(N_F/2)]. \tag{33}$$

Then, (25) can be expressed as

$$V_\xi(e^{j\omega})=\frac{1}{M}\mathbf{e}(\omega,N_P)\mathbf{C}\mathbf{E}(\xi,\omega)\mathbf{h} \tag{34}$$

where

$$\mathbf{e}(\omega,N_P)=[e^{j\omega N_P/2}\ \ e^{j\omega(N_P/2-1)}\ \ \cdots\ \ e^{-j\omega N_P/2}], \tag{35}$$

N_P is the order of the lowpass prototype filter for the synthesis FB and assumed to be even, the matrix $\mathbf{E}(\xi,\omega)$ is as shown in (36), and

$$\mathbf{C}=\begin{bmatrix} c_1(-N_P/2) & c_2(-N_P/2) & \cdots & c_K(-N_P/2)\\ \vdots & \vdots & & \vdots\\ c_1(0) & c_2(0) & \cdots & c_K(0)\\ \vdots & \vdots & & \vdots\\ c_1(N_P/2) & c_2(N_P/2) & \cdots & c_K(N_P/2) \end{bmatrix}. \tag{37}$$

In (36),

$$a_{k\ell}(\xi,\omega)=\beta_{km_\ell}\cos(\theta_{km_\ell})e^{-j(\omega-2\pi\xi/M)m_\ell}, \tag{38}$$

$$b_{k\ell}(\xi,\omega)=\beta_{km_\ell}\sin(\theta_{km_\ell})e^{-j(\omega-2\pi\xi/M)m_\ell}, \tag{39}$$

for $\ell=1,2,\dots,K$, and $\mathbf{e}(\omega,N_F)$ is a row-vector of length N_F+1 obtained by replacing N_P in (35) with N_F. In (37), $c_k(n)$, $k=1,2,\dots,K$, $n=-N_P/2,\dots,0,\dots,N_P/2$, are the impulse response coefficients of the synthesis filters $C_k(e^{j\omega})$. Using (34), we can rewrite (29) and (30) as

$$\mathcal{P}_0=\frac{1}{M^2}\mathbf{h}^T\mathbf{S}_0\mathbf{h}-\frac{2}{M^2}\mathbf{u}_0\mathbf{h}+\frac{1}{M^2} \tag{40}$$

and

$$\mathcal{P}_\xi=\frac{1}{M^2}\mathbf{h}^T\mathbf{S}_\xi\mathbf{h} \tag{41}$$

respectively, with

$$\mathbf{S}_\xi=\frac{1}{2\pi}\int_\Omega \mathbf{E}^\dagger(\xi,\omega)\mathbf{C}^T\mathbf{e}^\dagger(\omega,N_P)\mathbf{e}(\omega,N_P)\mathbf{C}\mathbf{E}(\xi,\omega)\,\mathrm{d}\omega,\quad \Omega\in\Omega_{r_i,\xi}, \tag{42}$$

$\xi=0,1,\dots,M-1$, and

$$\mathbf{u}_0=\frac{1}{2\pi}\int_\Omega \mathrm{Re}\{\mathbf{e}(\omega,N_P)\mathbf{C}\mathbf{E}(0,\omega)\}\,\mathrm{d}\omega,\ \ \Omega\in\Omega_{r_i,0}. \tag{43}$$

The analysis filter coefficients $\mathbf{h}$, which minimize the error power function in (28), can be determined by solving $\partial\mathcal{P}/\partial\mathbf{h}=0$ which gives

$$\mathbf{h}=\left[\sum_{\xi=0}^{M-1}\mathbf{S}_\xi\right]^{-1}\mathbf{u}_0^T. \tag{44}$$

[4]In this paper, to simplify derivations, we assume that all filters are noncausal. The designed filters can be easily made causal by adding suitable delays.

$$\mathbf{E}(\xi,\omega) = \begin{bmatrix} a_{11}(\xi,\omega)\mathbf{e}(\omega,N_F) & b_{11}(\xi,\omega)\mathbf{e}(\omega,N_F) & \cdots & a_{1K}(\xi,\omega)\mathbf{e}(\omega,N_F) & b_{1K}(\xi,\omega)\mathbf{e}(\omega,N_F) \\ a_{21}(\xi,\omega)\mathbf{e}(\omega,N_F) & b_{21}(\xi,\omega)\mathbf{e}(\omega,N_F) & \cdots & a_{2K}(\xi,\omega)\mathbf{e}(\omega,N_F) & b_{2K}(\xi,\omega)\mathbf{e}(\omega,N_F) \\ \vdots & \vdots & & \vdots & \vdots \\ a_{K1}(\xi,\omega)\mathbf{e}(\omega,N_F) & b_{K1}(\xi,\omega)\mathbf{e}(\omega,N_F) & \cdots & a_{KK}(\xi,\omega)\mathbf{e}(\omega,N_F) & b_{KK}(\xi,\omega)\mathbf{e}(\omega,N_F) \end{bmatrix} \quad (36)$$

C. Design of Reconfigurable Reconstructors

In a reconfigurable reconstructor, first, the prototype filter for the cosine-modulated synthesis FB, is designed as outlined in Section VI-A. Further, the subfilters $F_\ell(z)$ and $G_\ell(z)$ in the analysis FB are designed and fixed based on the sampling instants. In applications where all the L possible combinations (L modes) of the K active subbands use the same set of sampling instants, during reconfiguration, it suffices to redetermine the complex constants $\mathbf{v}_k$ in (11). Following a least-squares approach similar to the one outlined in Section VI-B, the coefficients of the subfilters $F_\ell(z)$ and $G_\ell(z)$ for the reconfigurable reconstructor are then determined using

$$\mathbf{h} = \left[\sum_{\gamma=1}^{L}\sum_{\xi=0}^{M-1}\mathbf{S}_\xi^{(\gamma)}\right]^{-1}\left[\sum_{\gamma=1}^{L}\mathbf{u}_0^{(\gamma)}\right]^T \quad (45)$$

where

$$\mathbf{S}_\xi^{(\gamma)} = \frac{1}{2\pi}\int_\Omega \mathbf{E}^{(\gamma)\dagger}(\xi,\omega)\mathbf{C}^T\mathbf{e}^\dagger(\omega,N_P)\mathbf{e}(\omega,N_P)\mathbf{C}\mathbf{E}^{(\gamma)}(\xi,\omega)\,\mathrm{d}\omega, \quad \Omega\in\Omega_{r_i,\xi}^{(\gamma)}, \quad (46)$$

and

$$\mathbf{u}_0^{(\gamma)} = \frac{1}{2\pi}\int_\Omega \mathrm{Re}\{\mathbf{e}(\omega,N_P)\mathbf{C}\mathbf{E}^{(\gamma)}(0,\omega)\}\,\mathrm{d}\omega, \quad \Omega\in\Omega_{r_i,0}^{(\gamma)}. \quad (47)$$

Here, $\Omega_{r_i,0}^{(\gamma)}$, $\gamma\in[1,2,\ldots,L]$, $r_i\in[0,1,\ldots,M-1]$, $i=1,2,\ldots,K$, represent the K active subband locations corresponding to the γth combination and $\Omega_{r_i,\xi}^{(\gamma)}$, $\xi = 1,\ldots,M-1$ represent their shifted versions which fall into the band $[-\pi,\pi]$. The matrix $\mathbf{E}^{(\gamma)}(\xi,\omega)$ is obtained by replacing $a_{k\ell}(\xi,\omega)$ and $b_{k\ell}(\xi,\omega)$ in (36) with $a_{k\ell}^{(\gamma)}(\xi,\omega)$ and $b_{k\ell}^{(\gamma)}(\xi,\omega)$, respectively, where

$$a_{k\ell}^{(\gamma)}(\xi,\omega) = \beta_{km_\ell}^{(\gamma)}\cos\left(\theta_{km_\ell}^{(\gamma)}\right)e^{-j(\omega-2\pi\xi/M)m_\ell} \quad (48)$$

and

$$b_{k\ell}^{(\gamma)}(\xi,\omega) = \beta_{km_\ell}^{(\gamma)}\sin\left(\theta_{km_\ell}^{(\gamma)}\right)e^{-j(\omega-2\pi\xi/M)m_\ell}. \quad (49)$$

The values for the constants $\beta_{km_\ell}^{(\gamma)}$ and $\theta_{km_\ell}^{(\gamma)}$ depend on the location of the active subbands in the γth combination and are determined using matrix inversion as explained in Section IV-B.

D. Design Complexity

Splitting the reconstructor design into two parts, as discussed above, makes it feasible to design and implement a reconfigurable reconstructor, especially for larger M. This is exemplified using a design example in Section VII. During reconfiguration, the proposed reconstructor can be reconfigured online by inverting a single $K\times K$ matrix if all modes use the same set of sampling instants. If each mode uses a different set of sampling instants, during reconfiguration, the reconfiguration requires only one additional $2K(N_F+1)\times 2K(N_F+1)$ matrix inversion. In contrast, for the straightforward scheme [7], the reconfiguration involves inverting several $(N_A+1)\times(N_A+1)$ matrices where N_A is the order of each multi-level synthesis filter $A_\ell(z)$ in Fig. 2. Typically, $N_A > 2K(N_F+1)$ as can be seen from the examples in Section VII.

VII. Design Examples

Example 1: In this example, we assume that there are three active users with two possible combinations of active band locations. It is assumed that at any given time frame, the active frequency bands can be either $\{[3.2\text{–}4.8],[7.2\text{–}7.8],[11.2\text{–}11.8]\}\times\pi/16$ or $\{[3.2\text{–}3.8],[7.2\text{–}7.8],[11.2\text{–}12.8]\}\times\pi/16$. Further, it is assumed that the reconstructor should be designed such that aliasing terms are kept below -60 dB.

For a given combination of active band locations, the number of channels, K, required to implement the CNUS scheme will depend on the total number of granularity bands M. In this example, the number of granularity bands M is chosen so as to get the least implementation complexity for the reconstructor. In order to have practical filters, a transition band is included in each active granularity band and, depending on M, the percentage occupancy ρ (see Section VI-A) of a granularity band is assumed to be within 20–60%. As shown in Fig. 12, for the two possible combinations of active band locations assumed in this example, the least computational complexity is obtained with $M=32$. When the total bandwidth is divided into $M=32$ granularity bands, with the information containing frequency bands assumed in this example, only $K=8$ granularity bands are active at any given time frame. Thus, at any given time frame, the users can be allocated either the granularity bands $\{6\text{–}9,14,15,22,23\}$ or the bands $\{6,7,14,15,22\text{–}25\}$. For the above two possible combination of band locations (two modes), we used the sub-Nyquist sampling points, $m=0,3,5,14,16,19,21,30$, which ensures that $\mathbf{D}$ in (11) is an invertible matrix. The sampling instants were determined using the method in [29].

Based on the occupied frequencies and the active bands, the percentage band occupancy ρ of the lowpass prototype filter $P(z)$ is fixed at 20%. The prototype filter is designed to be a power-symmetric lowpass filter of order 386 with $\omega_c = 0.2\pi/64$ and $\omega_s = 1.8\pi/64$. It is found that, for the 16 subfilters, $F_\ell(z)$ and $G_\ell(z)$, a filter order $N_F = 14$ is sufficient to keep the aliasing terms below -60 dB.

In order to determine the coefficients of the multi-level synthesis filters in the straightforward scheme in [7], we used

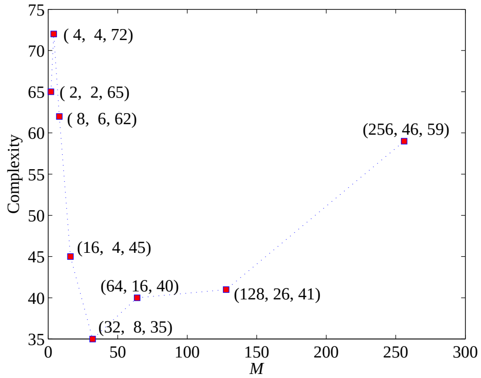

Fig. 12. Example 1: Computational complexity $\mathcal{C}_{\text{prop}}$ vs. M for the two possible active frequency band combinations $\{[3.2\text{–}4.8], [7.2\text{–}7.8], [11.2\text{–}11.8]\} \times \pi/16$ and $\{[3.2\text{–}3.8], [7.2\text{–}7.8], [11.2\text{–}12.8]\} \times \pi/16$. The numbers within parenthesis represent $(M, K, \mathcal{C}_{\text{prop}})$.

TABLE I
EXAMPLE 1: COMPLEXITY COMPARISON.

Reconstructor	Complexity[5]		
	$\mathcal{C}$	$\mathcal{N}$	Reconfiguration
Straightforward	80	2544	Eight $[319 \times 319]$
Proposed	29	128	One $[8 \times 8]$

the time-varying reconstructor design method in [30] but with some of the impulse response coefficients set to zero due to the CNUS scheme. It is found that the straightforward scheme would require a reconstructor with eight synthesis filters of order $N_A = 318$.

Table I tabulates the reconstructor complexity when the specification in this example is implemented using the straightforward and the proposed reconstructor. As can be seen from Table I, the proposed reconstructor offers significant reduction in complexity due to the efficient realization in Fig. 1. It can be seen that during reconfiguration from one mode to the other, the proposed reconstructor requires significantly fewer multipliers to be updated online. The coefficients of these multipliers can be either determined offline and stored in a memory or determined online using a single 8×8 matrix inversion. In contrast, the straightforward scheme would require a larger memory or eight 319×319 online matrix inversions.

Figure 13 shows all the distortion and aliasing terms of the reconstructor for the two possible combinations of user band locations. It can be seen that, in the required bands, the aliasing terms are not greater than -60 dB which validates the reconfigurability between the two different combinations of user band locations. The reconfigurability of the reconstructor is illustrated in Figs. 14 and 15 by configuring it for one set of active band locations and using it to reconstruct a sub-Nyquist sampled multi-tone input with tones in the active band region. The spectrum without reconstruction in Figs. 14 and 15 corresponds to the spectrum of the sub-Nyquist sampled signal

[5] $\mathcal{C}$ and $\mathcal{N}$ represent the number of multiplications per corrected output sample and the number of multipliers to be updated during reconfiguration, respectively. The reconfiguration complexity is the number of online matrix inversions. For the straightforward reconstructor, since we assume a polyphase implementation, $\mathcal{C}$ is computed as in (23).

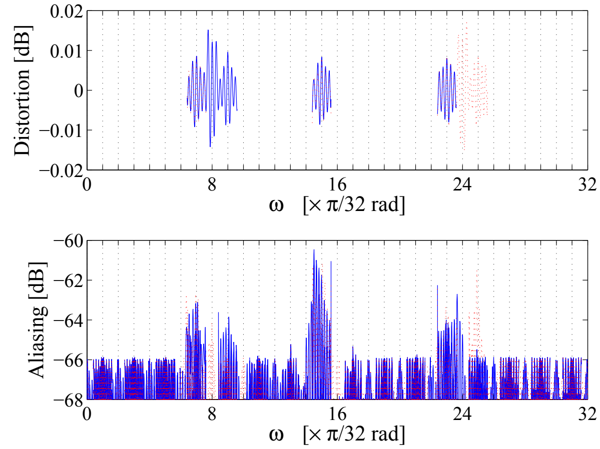

Fig. 13. Example 1: Distortion function $V_0(e^{j\omega})$ and aliasing functions $V_\xi(e^{j\omega})$, $\xi = 1, 2, \ldots, M-1$, for the active subband combinations $\{6\text{–}9, 14, 15, 22, 23\}$ (blue-continuous) and $\{6, 7, 14, 15, 22\text{–}25\}$ (red-dotted).

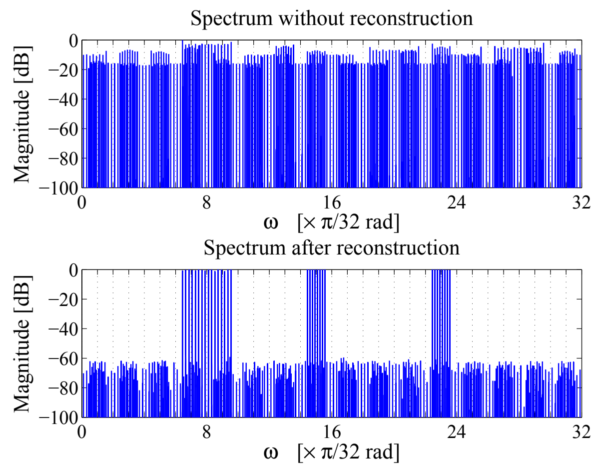

Fig. 14. Example 1: Reconstruction of sub-Nyquist sampled multi-tone signals with tones in the three user bands $\{[3.2\text{–}4.8], [7.2\text{–}7.8], [11.2\text{–}11.8]\} \times \pi/16$, after passing through the reconstructor.

with zeros inserted into the time instants where the samples are missing.

Example 2: This example illustrates that, for larger M, the proposed method provides even more significant savings in the design and implementation complexity of the reconstructor compared to the straightforward method that uses only synthesis FBs. This is in line with the complexity comparison in Section V-B. Here, we consider an example where the information containing frequency bands are $\{[3.21\text{–}3.82], [7.21\text{–}7.82], [20.21\text{–}21.82], [46.01\text{–}47.99], [54\text{–}55]\} \times \pi/64$ and the reconstructor should be designed to keep the aliasing terms below -40 dB. For the above frequency bands, the computational complexity of the reconstructor is least when $M = 128$ and $K = 18$. Consequently, the active granularity bands are $\{6, 7, 14, 15, 40\text{–}43, 91\text{–}96, 107\text{–}110\}$ with $\rho = 29\%$. Further, we use the sub-Nyquist sampling points $m =$

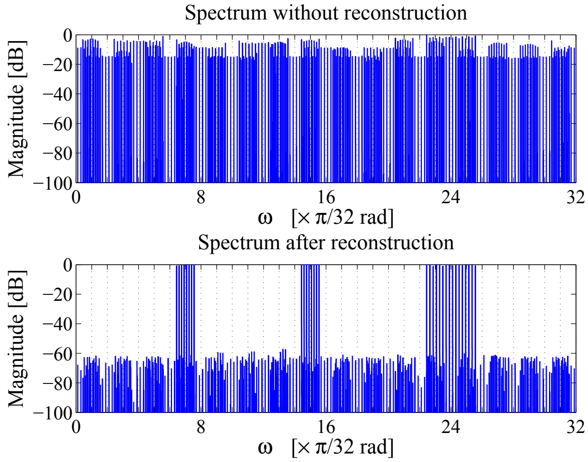

Fig. 15. Example 1: Reconstruction of sub-Nyquist sampled multi-tone signals with tones in the three user bands $\{[3.2\text{–}3.8], [7.2\text{–}7.8], [11.2\text{–}12.8]\} \times \pi/16$, after passing through the reconstructor.

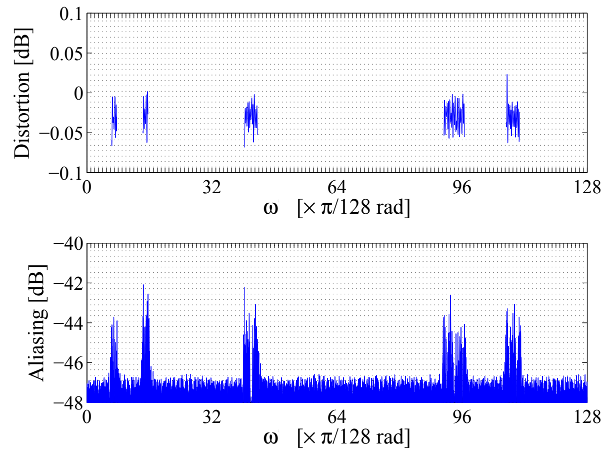

Fig. 16. Example 2: Distortion function $V_0(e^{j\omega})$ and aliasing functions $V_\xi(e^{j\omega})$, $\xi = 1, 2, \ldots, M-1$, for the active subbands, $\{6, 7, 14, 15, 40\text{–}43, 91\text{–}96, 107\text{–}110\}$.

TABLE II
EXAMPLE 2: COMPLEXITY COMPARISON.

Reconstructor	Complexity (see Footnote 5)		
	$\mathcal{C}$	$\mathcal{N}$	Reconfiguration
Straightforward	164	20934	18 [1163×1163]
Proposed	24	648	One [18×18]

$0, 1, 7, 8, 9, 32, 33, 34, 41, 55, 57, 73, 81, 84, 85, 86, 97, 126$, which were determined using the method in [29]. For the synthesis FB, a power-symmetric lowpass prototype filter of order 1162 is required to keep the aliasing terms below -40 dB at the output of the proposed reconstructor. The order of each of the 36 subfilters $F_\ell(z)$ and $G_\ell(z)$ in the analysis FB turned out to be 10. On the other hand, the straightforward reconstructor would require 18 synthesis filters where each filter has an order of around 1162.

Table II compares the complexity of the two reconstructors for the specification in this example. It can be seen that, for the given specification, the proposed reconstructor has around 70% lower computational complexity compared to the polyphase implementation of the straightforward reconstructor. Moreover, in the straightforward reconstructor, designing a synthesis FB with 20934 coefficients is quite hard if not impossible. Further, the proposed reconstructor can be reconfigured online through a single 18×18 matrix inversion. Online reconfiguration, however, is not feasible for the straightforward reconstructor due to the extremely large sizes of the matrices that need to be inverted. Figure 16 shows all the distortion and aliasing terms at the output of the proposed reconstructor designed to meet the requirements in this example.

VIII. CONCLUSION

In this paper, we proposed a reconfigurable reduced-complexity reconstructor for sub-Nyquist sampled sparse multi-band signals. The reconstructor was derived by expressing the reconstruction problem in terms of both analysis and synthesis FBs. We showed that the nonzero polyphase components of the bandpass filters in the analysis FB are generalized FD filters. Due to this, the analysis filters can be expressed in terms of a common set of fixed subfilters and a set of multipliers, thereby reducing the complexity. Moreover, since the filters in the synthesis FB are regular bandpass filters, further reduction in complexity was achieved by implementing these filters using a cosine-modulated FB. We also showed that, compared to the straightforward reconstructor, the proposed reconstructor makes it feasible to achieve order-of-magnitude reduction in the computational complexity. In addition, the proposed reconstructor provides significant reduction in the complexity of the online reconfiguration block as only the coefficients of the set of multipliers in the analysis FB have to be redetermined.

REFERENCES

[1] J. Singh, S. Ponnuru, and U. Madhow, "Multi-gigabit communication: the ADC bottleneck," in *Proc. IEEE Int. Conf. Ultra-Wideband*, Vancouver, BC, Sep. 2009, pp. 22–27.

[2] J. Selva, "Regularized sampling of multiband signals," *IEEE Trans. Signal Process.*, vol. 58, no. 11, pp. 5624–5638, Nov. 2010.

[3] M. Fleyer, A. Linden, M. Horowitz, and A. Rosenthal, "Multirate synchronous sampling of sparse multiband signals," *IEEE Trans. Signal Process.*, vol. 58, no. 3, pp. 1144–1156, Mar. 2010.

[4] M. Mishali and Y. Eldar, "Sub-Nyquist sampling," *IEEE Signal Process. Mag.*, vol. 28, no. 6, pp. 98–124, Nov. 2011.

[5] J. A. Tropp, J. N. Laska, M. F. Duarte, J. K. Romberg, and R. G. Baraniuk, "Beyond Nyquist: Efficient sampling of sparse bandlimited signals," *IEEE Trans. Inf. Theory*, vol. 56, no. 1, pp. 520–544, Jan. 2010.

[6] P. Feng and Y. Bresler, "Spectrum-blind minimum-rate sampling and reconstruction of multiband signals," in *Proc. IEEE Int. Conf. Acoust., Speech, Signal Process.*, vol. 3, Atlanta, GA , USA, May 1996, pp. 1688–1691.

[7] Y.-P. Lin and P. Vaidyanathan, "Periodically nonuniform sampling of bandpass signals," *IEEE Trans. Circuits Syst. II*, vol. 45, no. 3, pp. 340–351, Mar. 1998.

[8] P. P. Vaidyanathan and V. C. Liu, "Efficient reconstruction of band-limited sequences from nonuniformly decimated versions by use of polyphase filter banks," *IEEE Trans. Acoust., Speech, Signal Process.*, vol. 38, no. 11, pp. 1927–1936, Nov. 1990.

[9] R. Venkataramani and Y. Bresler, "Optimal sub-Nyquist nonuniform sampling and reconstruction for multiband signals," *IEEE Trans. Signal Process.*, vol. 49, no. 10, pp. 2301–2313, Oct. 2001.

[10] L. Berman and A. Feuer, "Robust patterns in recurrent sampling of multiband signals," *IEEE Trans. Signal Process.*, vol. 56, no. 6, pp. 2326–2333, Jun. 2008.

[11] A. Owrang, M. Viberg, M. Nosratinia, and M. Rashidi, "A new method to compute optimal periodic sampling patterns," in *Proc. IEEE Digital Signal Process. Workshop*, Sedona, AZ, USA, Jan. 2011, pp. 259–264.

[12] S. Tertinek and C. Vogel, "Reconstruction of nonuniformly sampled bandlimited signals using a differentiator–multiplier cascade," *IEEE Trans. Circuits Syst. I*, vol. 55, no. 8, pp. 2273–2286, Sep. 2008.

[13] K. M. Tsui and S. C. Chan, "New iterative framework for frequency response mismatch correction in time-interleaved ADCs: Design and performance analysis," *IEEE Trans. Instrum. Meas.*, vol. 60, no. 12, pp. 3792–3805, Dec. 2011.

[14] H. Johansson, "A polynomial-based time-varying filter structure for the compensation of frequency-response mismatch errors in time-interleaved ADCs," *IEEE J. Sel. Topics Signal Process.*, vol. 3, no. 3, pp. 384–396, Jun. 2009.

[15] K. M. Tsui and S. C. Chan, "A versatile iterative framework for the reconstruction of bandlimited signals from their nonuniform samples," *J. Signal Process. Syst.*, vol. 62, no. 3, pp. 459–468, Mar. 2011.

[16] A. Papoulis, "Generalized sampling expansion," *IEEE Trans. Circuits Syst.*, vol. 24, no. 11, pp. 652–654, Nov. 1977.

[17] Y.-M. Zhu, "Generalized sampling theorem," *IEEE Trans. Circuits Syst. II*, vol. 39, no. 8, pp. 587–588, Aug. 1992.

[18] A. K. M. Pillai and H. Johansson, "Efficient reconfigurable scheme for the recovery of sub-Nyquist sampled sparse multi-band signals," in *Proc. IEEE Global Conf. Signal Information Process.*, Austin, TX, USA, Dec. 2013, pp. 1294–1297.

[19] P. P. Vaidyanathan, "Multirate digital filters, filter banks, polyphase networks, and applications: a tutorial," *Proc. IEEE*, vol. 78, no. 1, pp. 56–93, Jan. 1990.

[20] ——, *Multirate Systems and Filter Banks*. Prentice-Hall, Englewood Cliffs, NJ, USA, 1993.

[21] H. Johansson and A. Eghbali, "Two polynomial FIR filter structures with variable fractional delay and phase shift," *IEEE Trans. Circuits Syst. I*, vol. 61, no. 5, pp. 1355–1365, May 2014.

[22] W. C. Black and D. A. Hodges, "Time interleaved converter arrays," *IEEE J. Solid-State Circuits*, vol. 15, no. 6, pp. 1022–1029, Dec. 1980.

[23] H. S. Malvar, "Extended lapped transforms: properties, applications, and fast algorithms," *IEEE Trans. Signal Process.*, vol. 40, no. 11, pp. 2703–2714, Nov. 1992.

[24] M. Bellanger, "On computational complexity in digital filters," in *Proc. Eur. Conf. Circuit Theory Design*, The Hague, The Netherlands, Aug. 1981, pp. 58–63.

[25] L. Wanhammar, *DSP Integrated Circuits*. Academic Press, 1999, ch. 11, pp. 461–530.

[26] O. Gustafsson, "Lower bounds for constant multiplication problems," *IEEE Trans. Circuits Syst. II*, vol. 54, no. 11, pp. 974–978, Nov. 2007.

[27] C. Creusere and S. Mitra, "A simple method for designing high-quality prototype filters for M-band pseudo QMF banks," *IEEE Trans. Signal Process.*, vol. 43, no. 4, pp. 1005–1007, Apr. 1995.

[28] f. harris, C. Dick, S. Seshagiri, and K. Moerder, "An improved square-root Nyquist shaping filter," in *Proc. Software Defined Radio Tech. Conf.*, Orange County, CA, USA, Nov. 2005, pp. 15–17.

[29] M. Rashidi and S. Mansouri, "Parameter selection in periodic nonuniform sampling of multiband signals," in *Proc. Int. Symp. Elect. Electron. Eng.*, Galiti, Romania, Sep. 2010, pp. 79–83.

[30] H. Johansson and P. Löwenborg, "Reconstruction of nonuniformly sampled bandlimited signals by means of time-varying discrete-time FIR filters," *EURASIP J. Advances Signal Process.*, vol. 2006, pp. 1–18, Jan. 2006.

Anu Kalidas M. Pillai (S'11) received the Bachelor of Technology degree in applied electronics and instrumentation engineering from University of Kerala, India, in 2002. He received the Master of Science degree in electrical engineering and the Doctoral degree in Communication Systems from Linköping University, Sweden, in 2011 and 2015, respectively. From 2002 to 2009, he was with Captronic Systems Pvt. Ltd., India, and was involved in the design and development of automated test equipments for automotive and aerospace applications. Currently, he is a researcher at the Division of Communication Systems at Linköping University. His research focus is on signal processing algorithms for parallel analog-to-digital interfaces.

Håkan Johansson (S'97–M'98–SM'06) received the Master of Science degree in computer science and the Licentiate, Doctoral, and Docent degrees in Electronics Systems from Linköping University, Sweden, in 1995, 1997, 1998, and 2001, respectively. During 1998 and 1999 he held a post doctoral position at Signal Processing Laboratory, Tampere University of Technology, Finland. He is currently Professor in Electronics Systems at the Department of Electrical Engineering of Linköping University. Prof. Johansson's research encompasses theory, design, and implementation of efficient and flexible signal processing systems for various purposes. He is one of the founders of the company Signal Processing Devices Sweden AB that sells advanced signal processing solutions. Prof. Johansson is the author or co-author of 4 books and some 170 international journal and conference papers. He is the co-author of three papers that have received best paper awards and he has authored two invited papers in IEEE Transactions and four invited chapters. Prof. Johansson has served as Associate Editor for IEEE Trans. on Circuits and Systems I and II, IEEE Trans. Signal Processing, and IEEE Signal Processing Letters. He is currently Associate Editor of IEEE Trans. on Circuits and Systems I and Area Editor of the Elsevier Digital Signal Processing journal, and a member of the IEEE Int. Symp. Circuits. Syst. DSP track committee.